Clim. Past, 22, 2031–2044, 2026
https://doi.org/10.5194/cp-22-2031-2026
© Author(s) 2026. This work is distributed under
the Creative Commons Attribution 4.0 License.

Climate of the Past
Open Access
EGU

Sea ice variability and links to East Siberian permafrost carbon remobilization during the last glacial-interglacial transition

Albin Eriksson[1,2], **Junjie Wu**[1,2,3], **Matt O'Regan**[2,4], **and Örjan Gustafsson**[1,2]

[1]Department of Environmental Science, Stockholm University, Stockholm, 11418, Sweden
[2]Bolin Centre for Climate Research, Stockholm University, Stockholm, 10691, Sweden
[3]Alfred Wegener Institute, Heimholtz Centre for Polar and Marine Research, Marine Geochemistry, 27570 Bremerhaven, Germany
[4]Department of Geological Sciences, Stockholm University, Stockholm, 10691, Sweden

Correspondence: Albin Eriksson (albin.eriksson@aces.su.se), Junjie Wu (junjie.wu@awi.de), and Örjan Gustafsson (orjan.gustafsson@aces.su.se)

Received: 27 April 2026 – Discussion started: 13 May 2026
Revised: 19 October 2026 – Accepted: 28 October 2026 – Published: 13 November 2026

Abstract. Sea ice plays a central role in the polar climate system, and its rapid decline in the Arctic over recent decades has altered surface albedo and the exchange of heat and gases between the ocean and atmosphere. Investigations of earlier warming events, such as the Preboreal/Early Holocene (PB/EH, 11–8 kyr B.P.), Bølling-Allerød (B/A, 14.7–12.9 kyr B.P.), and Dansgaard Oeschger event 3 (DO-3, 28–27.5 kyr B.P.), likely hold clues on climate system responses to changes in Arctic sea ice. This study explores the history of sea ice over the Southern Lomonosov Ridge and its potential relation to permafrost carbon remobilization. Sea ice conditions over the last 27 kyrs were reconstructed through a combination of the sea ice biomarker IP_{25} (Ice Proxy 25) and marine phytoplankton biomarkers (brassicasterol and dinosterol) from the chronologically well-constrained core 31-PC, sampled at the Southern Lomonosov Ridge during the SWERUS-C3 expedition in 2014. The reconstruction allowed for a direct comparison with previously published terrestrial organic carbon (terrOC) remobilization history from the same core. Our findings revealed a seasonal sea ice cover between 27–26 kyr B.P. after the DO-3 warm event, which likely caused more heat and moisture transport from ocean to land and strengthened permafrost thawing along the nearby coastline. A perennial sea ice cover then developed and persisted throughout the Last Glacial Maximum (LGM) to the Younger Dryas (YD), including the entire B/A warm period. Due to sea-level rise during Meltwater Pulse 1A (MWP 1A, 14.7–13.5 kyr B.P.), terrOC remobilization during B/A was rapid but its magnitude smaller when compared to PB and DO-3 in 31-PC, and other records from the Arctic. These records collectively suggest that sea-level rise, rather than sea ice conditions, exerts the primary control on coastal erosion during B/A, while we propose that the perennial sea ice cover may have limited wave-induced coastal erosion of the continental shelf bordering the Southern Lomonosov Ridge. A sharp reduction and breakup of the perennial sea ice was observed from the PB to the Early Holocene. Contrary to the B/A, Meltwater Pulse 1B during PB triggered significant coastal erosion and terrOC remobilization concurrent with the sea ice decline. The absence of sea ice in parallel to larger coastal erosion compared to B/A implies the role of waning sea ice in enhancing permafrost carbon mobilization along the coastline in this period. In accordance with sea ice records from other Arctic seas, the Holocene record exhibited a period of gradual sea ice expansion. Taken together, these findings highlight sea ice extent as a possible factor regulating coastal permafrost carbon remobilization during the last deglaciation.

1 Introduction

Sea ice in polar regions engages in the global climate system through albedo effects and the regulation of heat/gas exchange between the ocean and atmosphere (Solomon, 2006; Taylor et al., 2013; Duan et al., 2019). Additionally, sea ice

can influence the Atlantic Meridional Overturning Circulation (AMOC) by contributing with meltwaters and regulating the exposure of ocean water to sunlight (Sévellec et al., 2017). Thereby, it can affect both regional and even global climate processes. Recently, another coupling between sea ice extent and Arctic climate systems has been suggested. Observations and model simulations suggest that declining sea ice extent can lead to increased wave-induced coastal erosion due to a longer fetch and more frequent open water conditions (Overeem et al., 2011; Barnhart et al., 2014; Nielsen et al., 2020, 2024). Paleoclimate evidence implies that this could have been important in past climates with reduced sea ice conditions, enhancing permafrost thawing and subsequent greenhouse gas releases (Vaks et al., 2020). An extended sea ice cover can also reduce permafrost stability by affecting heat and moisture transport by shifting westerlies southward (Vandenberghe et al., 2012). Taken together, Arctic sea ice exerts significant control over key processes in the current and past climate, underscoring the need for further assessments of the role of sea ice in affecting climate-related processes.

Fundamentally, anthropogenic activities and associated greenhouse gas emissions are the main triggers for recent Arctic warming and sea ice retreat. However, the Arctic sea ice history beyond instrumental records can provide further clues on system functioning, including past effects and causes of Arctic climate change. Current paleoclimate evidence for Arctic sea ice is usually temporally limited to the Holocene or does not cover the full deglaciation process from the Last Glacial Maximum (LGM), particularly in the East Siberian Arctic (e.g, Fahl and Stein, 2012; Xiao et al., 2015; Hörner et al., 2016; Stein et al., 2017; Lin et al., 2025). Consequently, the role of sea ice in the global climate during periods of abrupt climate change requires further investigation. Specific molecular biomarkers of ice-associated phytoplankton, the highly branched isoprenoid alkenes (HBI) can be used as proxies to trace sea ice in the past (Belt et al., 2007). A commonly used HBI for sea ice reconstructions is IP_{25} (Ice Proxy with a 25 carbon atom skeleton). The application of IP_{25} is limited by two scenarios that result in the absence of IP_{25}: the absence of an ice-cover (which serves as the habitat for the sea ice diatoms that synthesise IP_{25}), and the presence of a permanent and thick sea ice cover that limits the light penetration through the ice and thereby the IP_{25} production (Müller et al., 2011). To address this issue, the PIP_{25} index (phytoplankton-IP_{25}) was introduced, where phytoplankton biomarkers such as brassicasterol and dinosterol indicate whether the absence of IP_{25} is caused by ice-free or permanent sea ice conditions (e.g., Müller et al., 2011; Xiao et al., 2013, 2015; Stein et al., 2017). Applications of the PIP_{25} index can provide a more comprehensive understanding of sea ice-climate interactions in the East Siberian Arctic during the last deglaciation.

The East Siberian Arctic holds extensive quantities of organic carbon (OC) within permafrost. The destabilization of this permafrost has historically, and continues to contribute to the significant remobilization of OC into the Arctic Ocean (e.g., Vonk et al., 2012; Köhler et al., 2014; Tesi et al., 2016; Martens et al., 2020, 2022; Wu et al., 2025; Vonk et al., 2025). The key mechanisms driving permafrost OC remobilization during the last deglaciation primarily include coastal erosion of the East Siberian Arctic Shelf due to sea level rise, active layer thawing, and subsequent riverine transport of OC (Tesi et al., 2016; Martens et al., 2020; Lin et al., 2025; Nicolas et al., 2025). Given the substantial OC reservoirs in Arctic permafrost and their potential impact on climate change, the understudied influence of sea ice dynamics on wave-induced coastal erosion warrants further investigation to better define terrestrial OC (terrOC) remobilization processes.

Permafrost carbon exhibits distinct isotopic characteristics depending on its formation time, which provide valuable clues for constraining carbon sources and their remobilization mechanisms. Ice Complex Deposits (ICD), also known as Yedoma, formed during the Late Pleistocene, are characterized by huge ice wedges and old radiocarbon ages, and are usually remobilized through thaw-induced coastal erosion (Vonk et al., 2012; Strauss et al., 2017). On the other hand, surficial permafrost consists of comparatively young radiocarbon and can be remobilized through processes such as active layer thawing and riverine erosion (Martens et al., 2020, 2022; Matsubara et al., 2022; Wu et al., 2025). By deconvoluting the source fingerprint of OC accumulating in the receptor sediments, it is possible to identify sources and mechanisms of permafrost carbon remobilization. Specifically, the source contribution can be investigated by analysing stable carbon isotopes ($\delta^{13}C$) to differentiate between marine and terrestrial OC (Semiletov et al., 2005; Martens et al., 2021). The relative contribution within the terrOC pool (such as surficial permafrost and erosion of deeper permafrost layers) can be further resolved by combining $\delta^{13}C$ with radiocarbon dating (^{14}C) given the age difference of the OC in these different permafrost pools (Gustafsson et al., 2011; Vonk et al., 2012; Karlsson et al., 2016; Wild et al., 2019; Martens et al., 2022). To further investigate mechanisms of remobilization, terrigenous biomarkers (sterols, lignin etc) can trace the input of terrestrial OC (terrOC) and provide further information about the origin of OC (Kremer et al., 2018; Tesi et al., 2016; Bröder et al., 2018; Matsubara et al., 2022). In summary, the carbon isotopic characteristics combined with terrigenous biomarkers enables source tracing of the sedimentary OC input, and the potential mobilization mechanisms.

In this study, we aim to investigate the sea ice history around the Southern Lomonosov Ridge to better understand sea ice changes during periods of abrupt climate change and their impacts on the remobilization of terrOC along permafrost coastlines. We utilized the well-characterized sediment core 31-PC from the Southern Lomonosov Ridge, located off the Laptev and East Siberian Seas (Fig. 1; Muschitiello et al., 2020; Martens et al., 2020). By reconstructing the sea ice history over the last 27 kyrs using IP_{25} and the

PIP_{25} index, we provide a detailed temporal record. Additionally, we incorporate findings from an isotope-based carbon source apportionment study on the same core (Martens et al., 2020) to explore the connection between sea ice and permafrost carbon remobilization.

2 Methods

2.1 Material and study area

During the SWERUS-C3 expedition in 2014 on the Swedish icebreaker *Oden*, an eight-meter-long piston core (31-PC) was obtained at 1120 m depth on the Southern Lomonosov Ridge (79.91° N, 143.23° E, Fig. 1). Due to disturbance of the surface sediments during the piston coring processes, surface sediment, representing the top of the core was used from multicore 31-MUC, sampled at the same location. The chronology of core 31-PC was established through a combination of bulk radiocarbon dating and stratigraphic correlation with Greenland ice-core records, resulting in an age-model covering the last 27 kyr (Muschitiello et al., 2020; Martens et al., 2020). The age-model was developed using a Markov Chain Monte Carlo algorithm to probabilistically align variations in sediment porosity with $\delta^{18}O$ records from Greenland ice cores, with eight bulk radiocarbon ages providing maximum age constraints. The age-model development is described in detail in Muschitiello et al. (2020). Sedimentation rates in 31-PC were on average $41 \pm 24\,cm\,kyr^{-1}$, apart from the past 9 kyr where they were lower ($15\,cm\,kyr^{-1}$; Muschitiello et al., 2020). The sampling location on the intersection between the Siberian continental margin and the Southern Lomonosov Ridge enabled sea ice reconstructions encompassing parts of the East Siberian- and Laptev Sea. Additionally, the sampling location enabled quantification of fluvially transported inland PF-C from the Lena River throughout the last deglaciation, including the Holocene. Notably, the core site was adjacent to ICD PF on the continental shelf, which formed during low sea levels and exposed deposits that are now submerged as subsea permafrost. This makes the core site an important receptor for terrOC from past shelf flooding and coastal erosion of the continental margin.

2.2 Lipid Biomarkers

The biomarker analyses were carried out following the method initiated by Belt et al. (2012), with minor modifications. Briefly, freeze-dried sediment samples were homogenised and ground to fine powders, followed by additions of 20 µL of 7-hexylnonadecane ($0.00465\,\mu g\,\mu L^{-1}$), 9-octylheptadec-8-ene ($0.00535\,\mu g\,\mu L^{-1}$), and androstanol ($0.45\,\mu g\,\mu L^{-1}$), respectively, as internal standards to correct for analyte losses during the laboratory procedure. Lipid extraction was performed on the sediments with saponification using KOH (5 %, MeOH / H_2O: 9/1, v/v; KOH ≥ 85 % purity; MeOH ≥ 99.9 % purity), heating for 1 h at 70 °C. The saponified compounds were then extracted by repeated liquid-liquid extractions with hexane after vortexing and centrifugating the samples. Condensed extracts were eluted into a non-polar (using 6 mL *n*-hexane) and a polar fraction (using 6 mL DCM / MeOH, 1 : 1, v/v) through open-column chromatography with 1 % H_2O deactivated silica gel (63–200 µm; Supelco) as the stationary phase.

Before instrumental analyses, the polar fraction was derivatized with N, O-Bis (trimethylsilyl) trifluoroacetamide (BSTFA) at 70 °C for 1 h. Both polar and non-polar fractions were analysed using gas chromatography-mass spectrometry (GC-MS) (GC-MS 7820-A, Agilent Technologies USA). Non-polar compounds were analysed in splitless mode using single ion monitoring mode (SIM), starting at a temperature of 40 °C, ramping up $10\,°C\,min^{-1}$ up to a maximum temperature of 300 °C for 10 min. To minimize potential carryover, a one-minute post-run at 305 °C was conducted for each sample. The polar fraction was analysed in splitless mode using total ion current mode (TIC), with a starting temperature of 60 °C held for one minute, followed by a 10 °C per minute temperature ramp to a maximum temperature of 310 °C, maintained for 16 min.

Identification of IP_{25} was based on the retention times of the compound in reference sediments provided by Professor Simon Belt (University of Plymouth). To ensure accurate identification of IP_{25}, the reference sediment and subsamples of 31-PC were first analyzed in full scan mode before SIM analysis. The target sterol compounds were identified based on the mass fragmentation pattern, and monitored through selective ion chromatograms, m/z 348, 470, 472, 486, 500 (androstanol, brassicasterol, campesterol, β-sitosterol, and dinosterol). Quantifications of IP_{25} and sterols were based on the differences in instrumental mass spectral responses of the target compounds and the internal standards, following the method of Belt et al., (2012). The response factors were determined using external calibration curves of HBI reference sediment, and external standards of the target sterols (Sigma-Aldrich). Additionally, the PIP_{25}-indices (Eqs. 1 and 2) were calculated according to Müller et al. (2011).

$$PIP_{25} = \frac{[IP_{25}]}{[IP_{25}] + ([P] \times c)} \quad (1)$$

$$c = \frac{\text{mean}\,[IP_{25}]}{\text{mean}[P]} \quad (2)$$

where P is a phytoplankton biomarker (e.g., brassicasterol or dinosterol), and c is the concentration balance factor to account for concentration differences in IP_{25} and phytoplankton biomarkers (Müller et al., 2011). Biomarker fluxes were determined by multiplying analyte concentrations with the dry bulk density and sedimentation rate in each slice of the sediment core following the approach of Martens et al. (2020). The limit of detection (LOD) for each biomarker was experimentally determined for each biomarker through external calibration curves of reference sediments (IP_{25}) and

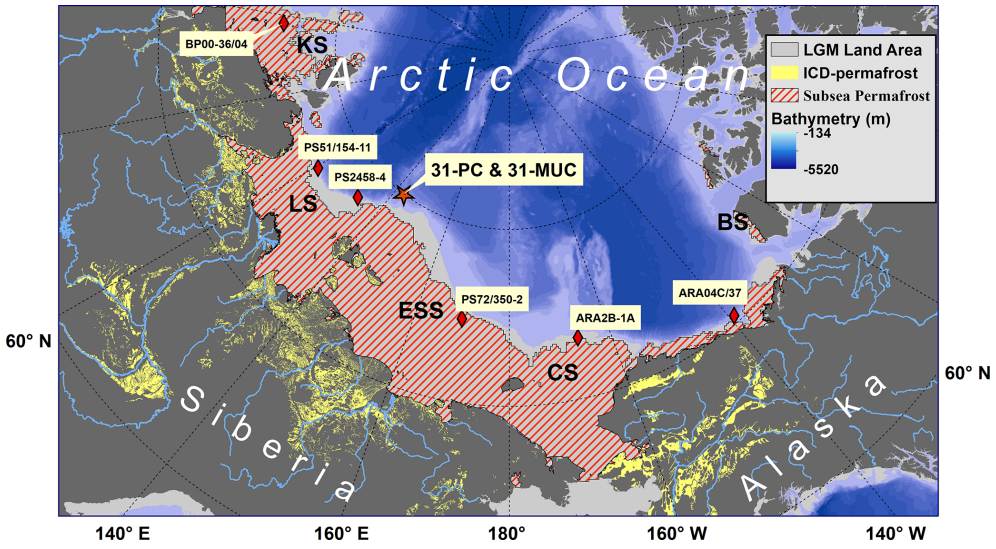


Figure 1. Sampling location of 31-PC and 31-MUC are indicated with a star marker. Other paleorecords of sea ice reconstruction discussed in this study are indicated with red rhombic markers. The current shelf seas of the Kara Sea (KS), Laptev Sea (LS), the East Siberian Sea (ESS), Chukchi Sea (CS), and Beaufort Sea (BS) are clarified with abbreviations. Bathymetry was applied using IBCAO version 4.2 (Jakobsson et al., 2020). The light-gray areas indicate land during the last glacial maximum (LGM), which were flooded during the last deglaciation. Yellow areas are contemporary land regions covered by ICD-permafrost (Strauss et al., 2022), and red lines display subsea permafrost in the contemporary Arctic (Overduin et al., 2019). Contemporary Arctic rivers are displayed as light blue lines.

sterols (external standards) according to Eq. 3.

$$\mathrm{LOD} = 3.3 \times \mathrm{SD}_{xy}/b \tag{3}$$

where SD_{xy} represents the residual standard deviation of the calibration curve and b is the slope of the calibration curve.

2.3 Carbon characteristics

The stable carbon isotope ratio (δ^{13}C-OC) in the surface sediment of 31-MUC was determined using an elemental analyser coupled to an isotopic ratio mass spectrometer (EA-irMS) following the procedure of Martens et al. (2020). The radiocarbon (Δ^{14}C) content of OC in 31-MUC was analysed through accelerator mass spectrometry at the Tandem Laboratory, Uppsala University. The other carbon isotopic composition and radiocarbon ages of OC in 31-PC were already published and re-used from Martens et al. (2020). However, new pre-depositional ages of the OC were employed in this study, now with the ages further corrected for atmospheric Δ^{14}C changes, according to Intcal20 (Reimer et al., 2020). The radiocarbon of OC at the time of deposition ($\Delta^{14}C_{\mathrm{initial}}$) was calculated through Eq. (4) (Schefuß et al., 2016).

$$\Delta^{14}C_{\mathrm{initial}} = (F^{14}C e^{\lambda t} - 1) \times 1000‰ \tag{4}$$

where $F^{14}C$ is the fraction modern carbon, t is the time of deposition, and λ the decay constant for radiocarbon. Furthermore, the pre-depositional age (years) was subsequently corrected through Eq. (5) (Schefuß et al., 2016).

$$\text{Pre-depositional age} = -8033 \times \ln\left[\frac{1 + \frac{(\Delta^{14}C_{\mathrm{initial}}}{1000}}{1 + \frac{\Delta^{14}C_{\mathrm{atm}}}{1000}}\right] \tag{5}$$

3 Results

In the core-bottom ∼27 kyr B.P., high concentrations and fluxes of marine and terrestrial biomarkers were observed. After the DO-3 (28–27.5 kyr B.P., Dansgaard et al., 1993) around ∼26.6–27 kyr B.P., the concentrations of IP_{25} (0.20–0.36 µg gOC^{-1}), dinosterol (7.60–24.8 µg gOC^{-1}), and brassicasterol were elevated compared to the rest of 31-PC (23.5–30.6 µg gOC^{-1}; Figs. 2 and 3). Concurrently, high fluxes of dinosterol (52.2–170.9 µg m^{-2} yr^{-1}) and brassicasterol (179.4–270.6 µg m^{-2} yr^{-1}; Fig. 2) were present. The PIP_{25} indices during this period ranged from approximately 0.2–0.4 (Fig. 2). Moreover, the aftermath of DO-3 was marked by high fluxes and concentrations of campesterol (181.5–269.5 µg m^{-2} yr^{-1}; 25.2–43.7 µg gOC^{-1}) and β-sitosterol (462.6–579.8 µg m^{-2} yr^{-1}; 66.7–84.5 µg gOC^{-1}). Around 26.5 kyr B.P., the fluxes and concentrations of these biomarkers diminished toward the LGM, with a concurrent abrupt increase in PIP_{25} (Figs. 2, 4 and 5).

From the LGM to around 11 kyr B.P., IP_{25}, dinosterol and brassicasterol declined to non-detectable levels, with only occasional low concentrations of dinosterol and brassicasterol (Figs. 2 and 3). Consequently, no PIP_{25} indices are

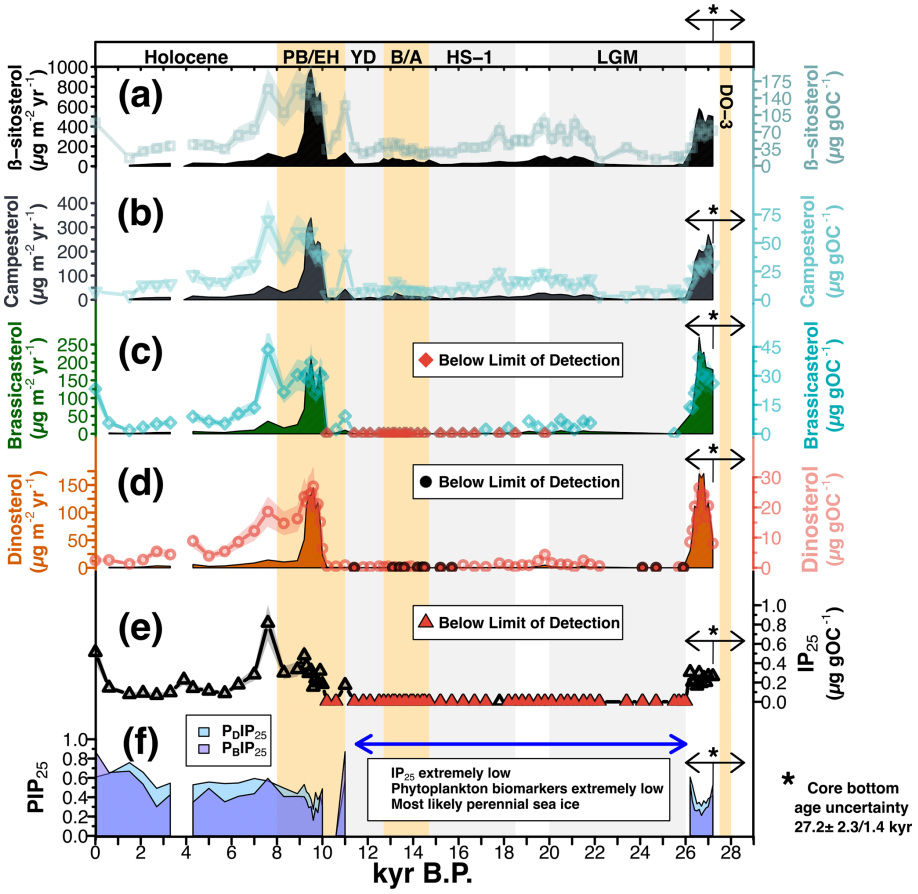


Figure 2. Biomarker fluxes and concentrations recorded in 31-PC ($\mu g\,m^{-2}\,yr^{-1}$; $\mu g\,gOC^{-1}$). Red filled markers indicate concentrations below the limit of detection, and the shaded regions around datapoints represent the uncertainty range of biomarker concentrations, based on the relative standard deviation of the internal standard recoveries. The black arrows at 27.2 kyr B.P. represent the age uncertainty (90 % confidence) in the core-bottom (Muschitiello et al., 2020). **(a)** β-sitosterol fluxes (dark brown), and concentrations (light blue-green). **(b)** Campesterol fluxes (dark gray) and concentrations (turquoise). **(c)** Brassicasterol fluxes (green), and concentrations (light blue). **(d)** Dinosterol fluxes (orange), and concentrations (light purple). **(e)** IP_{25} concentrations (black). **(f)** PIP25 indices, the darker shade of blue indicates P_BIP_{25}, and the lighter shade P_DIP_{25}. The interval 11–26 kyr B.P., is not displayed due to IP_{25} and brassicasterol remaining below the limit of detection or in extremely low concentrations, yielding unreliable PIP_{25} indices.

reported for this period (Fig. 2). Similarly, the fluxes and concentrations of campesterol and β-sitosterol remained relatively low from the LGM until 11 kyr B.P, with only minor increases noted around ~ 17–21 kyr B.P., and during B/A (Fig. 2).

Following a long period of non-detectable IP_{25} and extremely low concentrations of marine biomarkers extending between ~ 26–11 kyr B.P., the biomarker input abruptly shifted. In the PreBoreal and early Holocene (PB/EH) the highest concentrations of IP_{25} (0.19–0.39 μg gOC^{-1}), dinosterol (6.0–25.3 $\mu g\,gOC^{-1}$) and brassicasterol (20.7–37.0 $\mu g\,gOC^{-1}$) were observed (Figs. 2 and 3). The PIP_{25} indices during this period fluctuated between approximately 0.14 and 0.54 (Fig. 2). Moreover, the PB/EH marked elevated fluxes of these phytoplankton tracing biomarkers (Fig. 3). Parallel to the algal biomarker increases, the terrestrial biomarker fluxes and concentrations of campesterol (6.86–338.3 $\mu g\,m^{-2}\,yr^{-1}$; 6.41–59.7 $\mu g\,gOC^{-1}$) and β-sitosterol (61.2–976.9 $\mu g\,m^{-2}\,yr^{-1}$; 34.2–172.3 $\mu g\,gOC^{-1}$) were amplified during the PB/EH (Fig. 2).

As the Holocene progressed, the initially high fluxes and concentrations of IP_{25}, dinosterol, and brassicasterol gradually diminished, though a notable increase occurred around ~ 7–8 kyr B.P., followed by a gradual decline until ~ 1 kyr B.P. (Fig. 2). Correspondingly, the PIP_{25} indices gradually increased towards modern conditions (Fig. 2). In the mid-late Holocene, both campesterol and β-sitosterol exhibited decreases in concentrations and fluxes, with the exception of amplified levels around ~ 4 kyr B.P. and in the modern core-top sample (~ 0 kyr B.P.; Fig. 2).

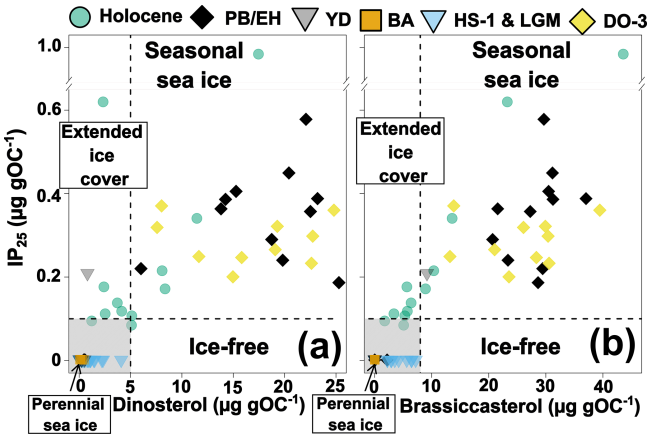


Figure 3. Sea ice distribution across the 27 kyrs recorded in 31-PC. Yellow diamond markers display the aftermaths of DO-3 (27–27.2 kyr B.P.), orange rectangular markers B/A, and black diamond markers the PB/EH. Inverted triangles show stadial conditions, and green circles indicate the Holocene. Black dashed lines distinguish the different extent of sea ice coverage.

4 Discussion

4.1 Seasonal sea ice and enhanced terrOC transport during the DO-3 interstadial

The Dansgaard-Oeschger (DO) events are characterized by rapid increases in atmospheric and sea surface temperatures, along with significant changes in hydrology (Dansgaard et al., 1993; Jensen et al., 2018). Given the age model uncertainty, the DO-3 event (28–27.5 kyr B.P.), or the aftermath of it, is likely captured at the base of 31-PC (spanning $27.2 \pm 2.3/-1.4$ kyr B.P., 90 % confidence interval; Muschitiello et al., 2020; Fig. 3). The relatively low PIP_{25} during this time suggest that the DO-3 likely led to approximately ∼ 1 kyr of seasonal sea ice cover, persisting until the transition into the LGM at 26 kyr B.P. This contrasts with earlier findings from the Southern Lomonosov Ridge (PS2767-4) that reported increased sea ice preceding the LGM (Xiao et al., 2015). However, this earlier study was based on a low-resolution core using a less well-constrained age model that was subsequently re-interpreted based on the improved dating of 31-PC (Muschitiello et al., 2020). Conclusively attributing seasonal sea ice cover during/after DO-3 to increased temperatures is still challenging, given that the onset of DO-3 is not captured in this record. Nevertheless, the amplified phytoplankton productivity following DO-3 was likely associated with seasonal sea ice cover and/or marginal ice zones. Nutrient input from melting sea ice may have contributed to the enhanced IP_{25}, dinosterol, and brassicasterol (Fig. 2: Belt, 2018), and the increased input of marine OC to the core location (Fig. 5; Martens et al., 2020). However, nutrient supply from terrestrial sources could also be an important contributor to the observation of increased productivity. As DO-3 progressed into its later stages, the increasing PIP_{25} values indicate an expanding sea ice cover approaching the LGM (Figs. 2 and 4).

Succeeding the DO-3, 31-PC recorded an abrupt increase in terrestrial biomarkers, consistent with the high input of OC observed in core 31-PC (Figs. 4 and 5; Martens et al., 2020). The terrestrial OC is characterized by young pre-depositional ages of ∼ 4–7 kyrs (Fig. 5). Accordingly, previous research attributed the significant input of terrestrial OC to active layer thawing, caused by warming during DO-3 (Martens et al., 2020). However, our records of reduced sea ice may suggest additional mechanisms causing active layer thawing, associated with heat and moisture transport during times of open water conditions. Specifically due to the proximity of the core location to the paleo-shoreline at the time (Fig. 1). The reduced sea ice after DO-3 may have led to higher air temperatures, which, combined with increased moisture sources, could result in heavy autumn snowfall. This snow could insulate the permafrost from low winter temperatures, leading to further thawing, as was displayed by Vaks et al. (2020). Consequently, the more frequent open water conditions observed in core 31-PC following DO-3, persisting for about 1 kyr or longer, may have contributed to the remobilization of permafrost carbon and observed enhancement of terrestrial OC input. Taken together, core 31-PC represents the first high-resolution record of sea ice history following DO-3 in this region, providing valuable insights into the sea ice impact on permafrost carbon remobilization.

4.2 Perennial sea ice and limited terrOC input during the LGM and HS-1 stadial

During the cold stadial of LGM and HS-1 (Heinrich Stadial-1), the concentrations of IP_{25} and marine phytoplankton biomarkers were below detection limits (Fig. 2), indicating the presence of permanent sea ice. The absence of these biomarkers suggests that thick sea ice inhibited the growth of open-water phytoplankton, but also hindered ice-algae by limiting light penetration through the ice. In contrast to studies that artificially set the PIP_{25} index to 1 in the absence of both sea ice and marine phytoplankton biomarkers, our records emphasize the absence of these biomarkers to highlight the presence of permanent sea ice (Fig. 2). The onset of perennial sea ice cover during the LGM is consistent with recently published proxy records from the central Arctic Ocean (Pavia et al., 2025). However, these results contrast with studies from the Laptev Sea, which suggest the existence of seasonal sea ice or even ice-free conditions during the HS-1 (Hörner et al., 2016; Fahl and Stein, 2012). Thus, the different sea ice conditions between the Southern Lomonosov Ridge and the nearby Laptev Sea may be attributed to the influence of Atlantic Water (Bradley and England, 2008), but it should be noted that the differences in sea ice cover can also be explained by the presence of polynyas in the Laptev Sea (Taldenkova et al., 2013). It is possible that this warm cur-

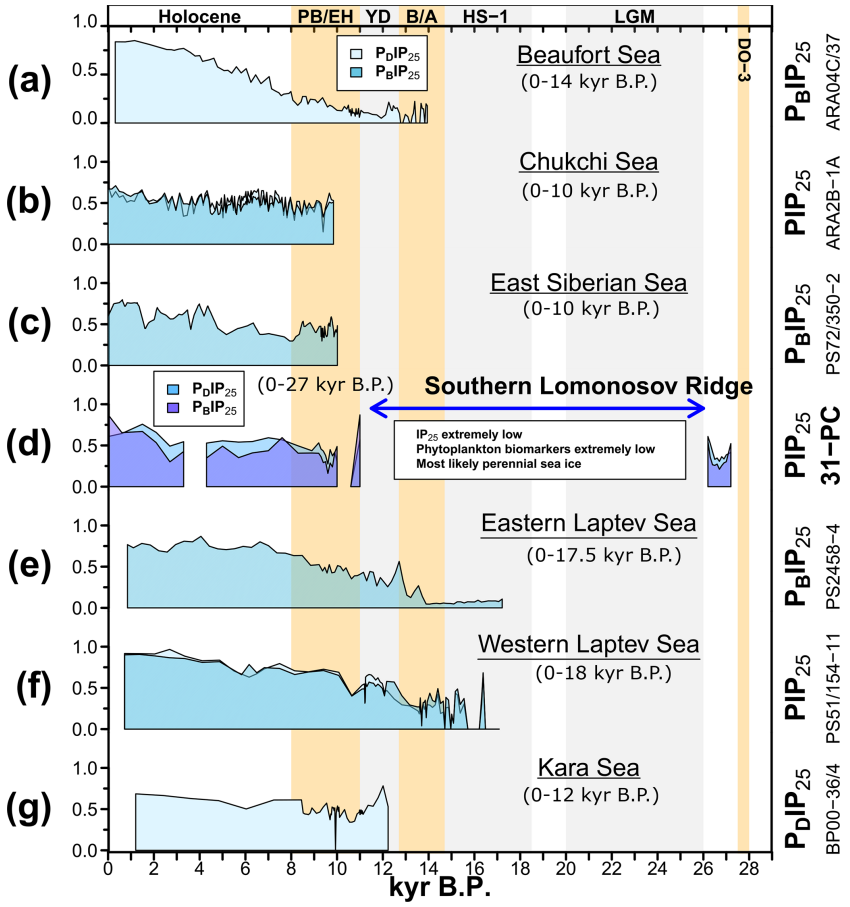


Figure 4. Temporal distribution of reconstructed PIP_{25} sea ice in marine sediment cores across the Arctic Ocean during the last 27.2 kyr B.P. **(a)** P_DIP_{25} in a Beaufort Sea sediment core covering the last 14 kyr (Wu et al., 2020). **(b)** Chukchi Sea sediment core covering the last 10 kyr (Stein et al., 2017). **(c)** P_BIP_{25} in an East Siberian Sea sediment core covering the last 10 kyr (Stein et al., 2017). **(d)** The 31-PC record covering the last 27.2 kyr. The interval 11–26 kyr B.P., is not displayed due to IP_{25} and brassicasterol remaining below the limit of detection or in extremely low concentrations, yielding unreliable PIP_{25} indices (Fig. 2). **(e)** P_BIP_{25} in a nearby core from the Laptev Sea, covering the last 17.5 kyr (Fahl and Stein, 2012). **(f)** Western Laptev Sea sediment core covering the last 18 kyr (Hörner et al., 2016; Lin et al., 2025). **(g)** P_DIP_{25} in a Kara Sea sediment core covering the last 12 kyr (Hörner et al., 2018).

rent has reduced sea ice in the Laptev Sea, while the Southern Lomonosov Ridge and the adjacent East Siberian Sea were less affected by this warm inflow and maintained permanent sea ice (Xiao et al., 2015). This could also explain the near absence of pre-Holocene sediment records in the East Siberian Sea. However, further studies are necessary to validate this hypothesis.

The input of the terrestrial biomarkers campesterol and β-sitosterol was significantly reduced during the LGM and HS-1 (Fig. 2). Previous studies have attributed this decline to the stabilization of permafrost under the cold climate (Martens et al. 2020). After 26 kyr B.P., the decreasing pre-depositional age and low ICD-OC flux suggest that permanent sea ice may have acted as a barrier for transport of terrestrial matter to the study site. It is also worth noting that the presence of permanent sea ice likely reduced the fetch distance and wave activity, thereby protecting coastal areas from erosion and minimizing the input of older carbon sources such as those from ICD-PF. While limited coastal erosion was evident at the Southern Lomonosov Ridge site, a seasonal sea ice cover in the Western Laptev Sea resulted in a stronger input of terrestrial organic matter (Hörner et al., 2016) compared to 31-PC. During the HS-1, 31-PC was rather close to the coastline (75 km), indicating that the core should provide a record of coastal erosion of the continental margin and terrestrial export of organic matter. However, low fluxes of OC and terrestrial biomarkers were present in 31-PC (Figs. 2 and 5). In the Western Laptev Sea, β-sitosterol and campesterol concentrations were around four times higher during the HS-1 (Hörner et al., 2016) compared to 31-PC. This highlights the role of perennial sea ice in limiting terrestrial carbon export during the HS-1 in 31-PC. Additionally, the proximity to the coastline of both cores captures how seasonal sea ice in the Western Laptev Sea permitted higher terrOC input

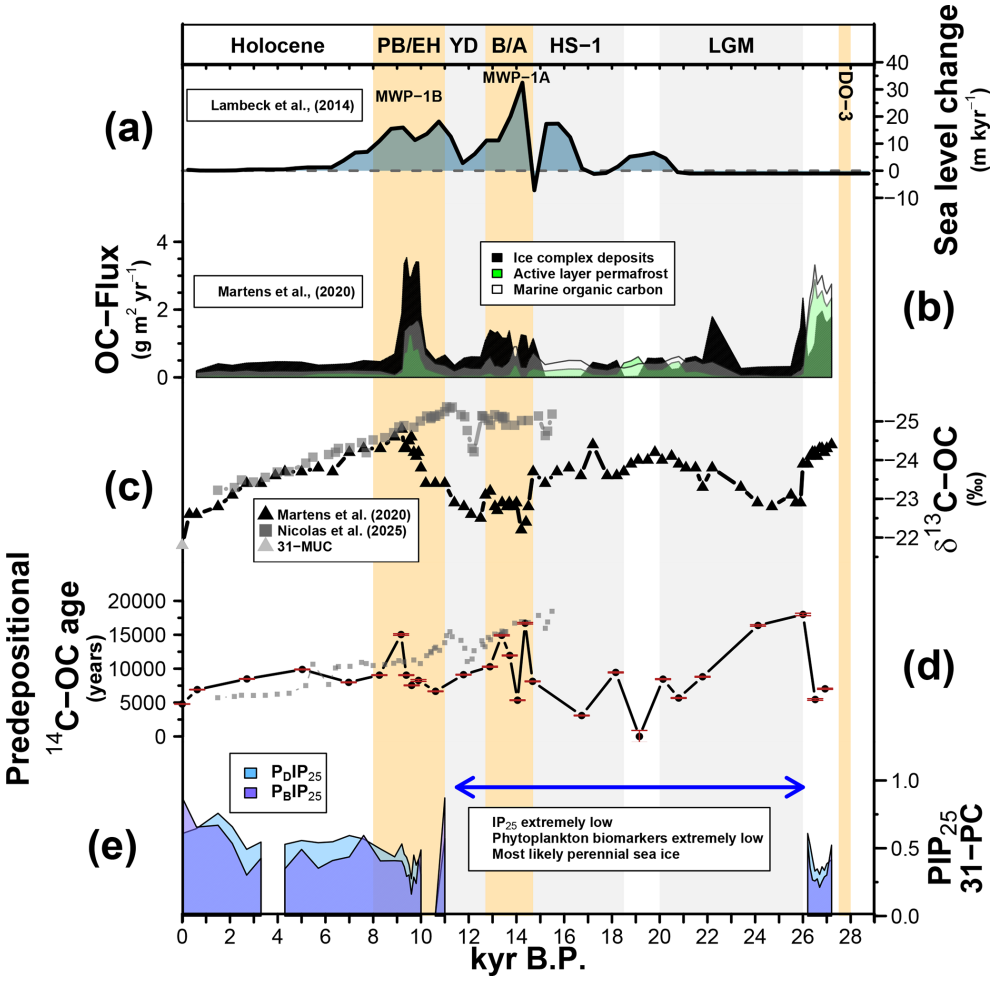


Figure 5. Carbon characteristics and PIP_{25} reconstructed sea ice using the 31-PC record. **(a)** The rate of sea level change ($m\,kyr^{-1}$) throughout the studied time-period (Lambeck et al., 2014). **(b)** Organic carbon fluxes ($g\,m^{-2}\,yr^{-1}$) based on source apportionments from Martens et al. (2020). The light green shading represents active layer (younger) permafrost, the darker shading the ice complex deposits formed during the Pleistocene and the white is marine organic carbon. **(c)** Stable isotopic signature (δ^{13}C-OC) of 31-PC from Martens et al. (2020), including the addition of the surface layer from 31-MUC $\sim$0 kyr B.P. Stable isotopic signature (δ^{13}C-OC) of Eastern Laptev Sea core PS2458-4 (Nicolas et al., 2025). **(d)** Recalculated predepositional age of ^{14}C-OC at the time of atmospheric carbon sequestration in 31-PC (Martens et al., 2020), with the red bars displaying the maximum and minimum estimate, and predepositional age of ^{14}C-OC in Eastern Laptev Sea core PS2458-4 (Nicolas et al., 2025). **(e)** PIP_{25} reconstructed sea ice with dinosterol (P_DIP_{25}) and brassicasterol (P_BIP_{25}) as the phytoplankton biomarkers. The blue arrow indicates the time when individual phytoplankton and IP_{25} were extremely low, yielding unreliable PIP_{25}-indices, see Fig. 3 for reference.

through coastal erosion. Conversely, perennial sea ice cover over the Southern Lomonosov Ridge limited erosion of the nearby continental margin.

During the LGM, the reduction of wave-induced coastal erosion is apparent despite the proximity to the ICD-coastline (Fig. 1). Interestingly, our record showed a minor increase in terrestrial biomarkers and brassicasterol between $\sim$19–22 kyr B.P., while such an increase was absent in dinosterol (Fig. 2). Given that brassicasterol may have lacustrine sources (Hörner et al., 2016), this increase may indicate a moderate rise in material from riverine input. However, the underlying cause of this increase remains unclear, especially considering the cold climate, presence of permanent sea ice (Fig. 2), and relatively stable sea levels (Lambeck et al., 2014).

4.3 Perennial sea ice persisting into the Younger Dryas with limited terrOC input during the Bølling-Allerød interstadial

During the YD stadial, and despite the warming climate of the B/A, the IP_{25} and open-water algae biomarkers remained undetectable, comparable to the levels observed during the LGM (Fig. 2). This suggests that permanent sea ice persisted

from the LGM until approximately 11 kyr BP. This sea ice condition contrasts with the patterns observed in the Kara Sea, Laptev Sea, and the Beaufort Sea, where the sea ice cover was reduced during the B/A and slightly increased during the YD, but generally remained seasonal (Fig. 4; Hörner et al., 2016, 2018; Fahl and Stein, 2012; Wu et al., 2020). Lin et al. (2025) proposed that during this time, Atlantic Water inflow inhibited sea ice formation in the Laptev Sea. Similar to the conditions during the LGM and HS-1. Therefore, the persisting sea ice cover in the Southern Lomonosov Ridge and Eastern Laptev Sea is possibly due to the less profound impact of warm Atlantic Water inflow to our study area.

While permanent sea ice persisted during the B/A, there was a modest increase in terrestrial input, coupled with a notable increase in the pre-depositional age of OC, reaching approximately 15 kyr (Figs. 2 and 5). This implies the involvement of additional mechanisms that remobilized older permafrost carbon. Typically, permanent sea ice is expected to reduce wave activity, thereby limiting coastal erosion, and to decrease heat and moisture transport, which reduces inland permafrost thawing (Barnhart et al., 2014; Vaks et al., 2020). Thus, the observed increase in permafrost carbon remobilization is likely linked to the shelf flooding induced by sea-level rise during the meltwater pulse 1A (MWP-1A; Lambeck et al., 2014; Martens et al., 2020). Indeed, profound sea level rise was observed in the nearby Laptev Sea during MWP-1A (Bauch et al., 2001). This indicates that permafrost carbon remobilization during the B/A was primarily influenced by sea-level rise and atmospheric warming, rather than by sea ice conditions at our study location. It is important to note that the magnitude of permafrost remobilization recorded in core 31-PC was moderate compared to the DO-3 and PB events, as well as compared to the Sea of Okhotsk, Bering Sea, North Pacific, and Beaufort Sea, where extensive remobilization during the B/A has been widely documented (Winterfeld, et al., 2018; Meyer et al., 2019; Wu et al., 2022). This suggests a significant role of the permanent sea ice limiting coastal erosion during B/A of the continental margin close to the Southern Lomonosov Ridge. Indeed, the OC-fluxes were much larger in 31-PC when seasonal sea ice was present after DO-3 and the PB (Figs. 2 and 5). Additionally, nearby cores in the Eastern (PS2458; Fahl and Stein, 2012) and Western Laptev Sea (PS51-154/11; Hörner et al., 2016) display open water/seasonal sea ice conditions concurrent to input of preaged OC/*n*-alkanoic acids, but in several orders of magnitude higher fluxes than in 31-PC (Fig. 5; Nicolas et al., 2025). This suggests that the presence of perennial sea ice at the Southern Lomonosov Ridge, similar to the HS-1, served as a barrier to limit the transport of terrestrial derived material to the core location, and that coastal erosion of the continental margin was limited close to the site. In contrast, regional variability was evident in the Laptev Sea, where seasonal sea ice permitted substantially greater transport of terrestrial organic carbon, partly facilitated by the sea ice conditions permitting more coastal erosion (Fahl and Stein, 2012; Hörner et al., 2016). Granted that permanent sea ice likely limited the transport of terrOC to the core site, the actual magnitude of terrOC input driven by sea-level rise in this region remains uncertain and warrants further investigation.

During the YD stadial, terrestrial input returned to low levels, comparable to the marine contributions as indicated by the marine phytoplankton biomarkers and carbon source apportionment (Fig. 2; Martens et al., 2020). Overall, the low terrestrial input and young pre-depositional age suggest that the cold climate of the YD likely contributed to the stabilization of permafrost, and the permanent sea ice may have had an additional effect on this stabilization.

4.4 Breakup of perennial sea ice and increased terrOC input during the Early Holocene

During the PB/EH transition, there was a marked increase in IP_{25} and marine phytoplankton biomarkers, with PIP_{25} values indicating the presence of seasonal sea ice (Fig. 3). Although the emergence of seasonal sea ice aligns with the warmer climate of this period (Shakun et al., 2012), large-scale Arctic sea ice records suggest that the elevated temperatures were not drivers of the breakup of permanent sea ice. This is evident from the observations that sea ice in regions like the Beaufort Sea and Laptev Sea was reduced during the cold deglaciation and expanded during the warm Early Holocene (Fig. 4; Wu et al., 2020; Fahl and Stein, 2012; Hörner et al., 2016). Instead, the transition was likely driven by summer solar insolation at 70° N reached its maximum during this time (Laskar et al., 2004; Stranne et al., 2014). Comparisons with sea ice records from the nearby Laptev Sea reveal contrasting patterns during the early Holocene: while sea ice over the Southern Lomonosov Ridge transitioned from permanent to seasonal sea ice, sea ice coverage in the Laptev Sea increased (Fig. 4; Hörner et al., 2016; Lin et al., 2025). This suggests that the solar insolation, rather than warm Atlantic Water, became the dominant factor influencing sea ice dynamics during this period.

During the PB/EH, there was a substantial increase in terrestrial biomarkers of campesterol and β-sitosterol, even surpassing levels observed during the DO-3 (Fig. 2). Source apportionment of OC suggest that most of the OC in 31-PC came from ICD at the time (Fig. 5; Martens et al., 2020). Due to cross-shelf transport of 0.6 to 2.6 kyr of the OC (Martens et al., 2020), the mobilization could be linked to coastal erosion driven by sea-level rise during the MWP-1B (Lambeck et al., 2014). This finding is consistent with massive permafrost carbon remobilization recorded in the Laptev Sea, Chukchi Sea, Beaufort Sea, Okhotsk Sea, Bering Sea, and North Pacific (Tesi et al., 2016; Martens et al., 2019; Wu et al., 2022; Winterfeld et al., 2018; Meyer et al., 2019; Lin et al., 2025). However, a role of concurrent sea ice reduction cannot be excluded. Seasonal sea ice can promote wave-induced coastal erosion of ICD by increasing fetch distance under frequent open water conditions (Barnhart et al., 2014). Additionally,

open water conditions can further elevate heat and moisture transport, potentially leading to deeper thaws of permafrost (Vaks et al., 2020). Therefore, it is plausible that sea-level rise and sea ice reduction acted synergistically to increase destabilization of coastal permafrost, although their relative contributions remain unclear.

4.5 Gradual buildup of extended sea ice during the Late-Mid Holocene

Following the rapid decline in sea ice cover during the PB/EH transition, the Mid-Late Holocene is characterized by relatively stable environmental conditions. Starting around 7.5 kyr B.P., phytoplankton and sea ice algae productivity gradually diminished, indicating a buildup of a more extended sea ice cover (Fig. 3). The trend of expanding Arctic sea ice towards the Late Holocene, as observed in our record, is consistent with findings from the Beaufort Sea, Kara Sea, Chukchi Sea, Laptev Sea, and East Siberian Sea (Fig. 5; Fahl and Stein, 2012; Hörner et al., 2016, 2018; Stein et al., 2017; Wu et al., 2020; Dong et al., 2022). Dong et al. (2022) found that the primary driver for mid-Holocene sea ice reduction in the East Siberian Sea was increased solar insolation, driving heat discharge from Arctic rivers. In accordance, the sea ice cover in our record as well as Dong et al. (2022) expanded in the Late Holocene, attributed to reduced summer insolation and resulting heat discharge from nearby rivers.

Coinciding with the expanding sea ice cover, the input of campesterol and β-sitosterol gradually decreased throughout the Holocene, implying a decline in terrOC contribution in tandem with reduced marine productivity (Figs. 2 and 4). This trend of minimal terrOC input and OC deposition is consistently observed in the Laptev Sea and East Siberian Sea (Tesi et al., 2016; Keskitalo et al., 2017; Martens et al., 2020). Although the OC input remained low during the Holocene, the relative influence of marine sources became more important towards the Late Holocene (Fahl and Stein, 2012; Martens et al., 2020). The terrOC remobilization of permafrost pools reduced, likely due to the relatively stable climatic conditions that did not trigger significant OC remobilization, as had occurred during earlier periods of rapid temperature rise.

5 Conclusions

This study reconstructed sea ice history over the past 27 kyrs at the Southern Lomonosov Ridge using the sea ice biomarker IP_{25} and open-water algae biomarkers brassicasterol and dinosterol, providing a comprehensive record that spans the late DO-3 and LGM through the deglaciation period. This work offers new insights into past sea ice variability and its controlling mechanisms. With emerging studies suggesting that sea ice can indirectly influence permafrost thaw and mobilization by modulating wave activity, heat, and moisture transport, we integrated our sea ice reconstruction with previously detailed investigations of permafrost carbon remobilization from the same core. The combined approach sheds light on the role of sea ice in influencing permafrost thaw under climate change. The key findings of this study are as follows:

1. The sea ice over the Lomonosov Ridge exhibited seasonal variability after the DO-3 interstadial, followed by the establishment of permanent sea ice persisting until 11 kyr BP. The breakup of this permanent sea ice occurred during the early Holocene, leading to a period of low sea ice concentrations, which then gradually increased through the mid-late Holocene.

2. Compared to sea ice records from the nearby Laptev Sea, the warm Atlantic water inflow likely played a primary role in the contrasting sea ice conditions between these two regions during the deglaciation: while the Lomonosov Ridge experienced permanent sea ice, the Western Laptev Sea was characterized by seasonal/ice-free conditions. The breakup of permanent sea ice during the early Holocene, followed by a subsequent expansion, is consistent with records from other parts of the Arctic Ocean, suggesting a predominant influence from solar insolation forcing during this period.

3. Permafrost carbon remobilization occurred after DO-3, during B/A, and PB/EH interstadials. The reduction in sea ice after DO-3 and PB/EH likely contributed to permafrost destabilization by modulating wave activity and heat/moisture transport, which further enhanced coastal erosion and inland permafrost thaw. In contrast, the moderate carbon remobilization observed during the B/A, compared to DO-3 and PB/EH, may indicate that permanent sea ice to some degree can protect the coastline, and limit coastal erosion of the continental margin. Therefore, the magnitude of permafrost-carbon remobilization could be attenuated by permanent sea ice serving as a barrier for terrOC transport to the marine realm, and by limiting the extent of coastal erosion.

Data availability. The supplementary dataset can be accessed on the Bolin Centre Database (https://doi.org/10.17043/eriksson-2026-31pc-biomarker-1, Eriksson et al., 2026).

Author contributions. The study was conceptualized by Ö.G and J.W. Sediment sampling was conducted by M.R. Laboratory work, methodology and creation of the first manuscript draft was made by A.E under supervision of J.W and Ö.G. All authors have contributed to data interpretation and writing of the manuscript.

Competing interests. The contact author has declared that none of the authors has any competing interests.

Disclaimer. Publisher's note: Copernicus Publications remains neutral with regard to jurisdictional claims made in the text, published maps, institutional affiliations, or any other geographical representation in this paper. The authors bear the ultimate responsibility for providing appropriate place names. Views expressed in the text are those of the authors and do not necessarily reflect the views of the publisher.

Acknowledgements. We thank the crew onboard the Swedish icebreaker *Oden* for the sampling of 31-PC. We also thank Dr. Francesco Muschitiello for the work on the age-model of 31-PC (Muschitiello et al., 2020), and Dr. Jannik Martens for conducting previous carbon geochemistry analyses (Martens et al., 2020). We further thank Dr. Wen Zhang for assisting with the analytical protocol, and Professor Simon Belt for providing reference sediments to enable quantifications of IP_{25}.

Financial support. This research has been supported by the Knut och Alice Wallenbergs Stiftelse (grant no. 2011.0027), the Vetenskapsrådet (grant nos. 621-2013-5297 and 621-2017-01601), and the European Research Council, FP7 Ideas: European Research Council (grant no. 695331).

The publication of this article was funded by the Swedish Research Council, Forte, Formas, and Vinnova.

Review statement. This paper was edited by Erin McClymont and reviewed by two anonymous referees.

References

Barnhart, K. R., Overeem, I., and Anderson, R. S.: The effect of changing sea ice on the physical vulnerability of Arctic coasts, The Cryosphere, 8, 1777–1799, https://doi.org/10.5194/tc-8-1777-2014, 2014.

Bauch, H. A., Mueller-Lupp, T., Taldenkova, E., Spielhagen, R. F., Kassens, H., Grootes, P. M., Thiede, J., Heinemeier, J., and Petryashov, V. V.: Chronology of the Holocene transgression at the North Siberian margin, Global Planet. Change, 31, 125–139, https://doi.org/10.1016/S0921-8181(01)00116-3, 2001.

Belt, S.: Source-specific biomarkers as proxies for Arctic and Antarctic sea ice, Org. Geochem., 125, 277–298, https://doi.org/10.1016/j.orggeochem.2018.10.002, 2018.

Belt, S. T., Massé, G., Rowland, S. J., Poulin, M., Michel, C., and LeBlanc, B.: A novel chemical fossil of palaeo sea ice: IP_{25}, Org. Geochem., 38, 16–27, https://doi.org/10.1016/j.orggeochem.2006.09.013, 2007.

Belt, S. T., Brown, T. A., Navarro Rodriguez, A., Cabedo Sanz, P., Tonkin, A., and Ingle, R.: A reproducible method for the extraction, identification, and quantification of the Arctic sea ice proxy IP_{25} from marine sediments, Anal. Methods, 4, 705–713, https://doi.org/10.1039/C2AY05728J, 2012.

Bradley, R. S. and England, J. H.: The Younger Dryas and the Sea of Ancient Ice, Quaternary Res., 70, 1–10, https://doi.org/10.1016/j.yqres.2008.03.002, 2008.

Bröder, L., Tesi, T., Andersson, A., Semiletov, I., and Gustafsson, Ö.: Bounding cross-shelf transport time and degradation in Siberian-Arctic land-ocean carbon transfer, Nat. Comm, 9, 806, https://doi.org/10.1038/s41467-018-03192-1, 2018.

Dansgaard, W., Johnsen, S. J., Clausen, H. B., Dahl-Jensen, D., Gundestrup, N. S., Hammer, C. U., Hvidberg, C. S., Steffensen, J. P., Sveinbjörnsdottir, A. E., Jouzel, J., and Bond, G.: Evidence for general instability of past climate from a 250-kyr ice-core record, Nature, 364, 218–220, https://doi.org/10.1038/364218a0, 1993.

Dong, J., Shi, X., Gong, X., Astakhov, A.S., Hu, L., Liu, X., Yang, G., Wang, Y., Vasilenko, Y., Qiao, S., Bosin, A., and Lohmann, G.: Enhanced Arctic sea ice melting controlled by larger heat discharge of mid-Holocene rivers, Nat. Commun., 13, 5368, https://doi.org/10.1038/s41467-022-33106-1, 2022.

Duan, L., Cao, L., and Caldeira, K.: Estimating Contributions of Sea Ice and Land Snow to Climate Feedback, Atmospheres, 124, 199–208, https://doi.org/10.1029/2018JD029093, 2019.

Eriksson, A., Wu, J., O'Regan, M., and Gustafsson, Ö.: Sea ice, phytoplankton and terrestrial biomarker fluxes/concentrations in sediment core 31-PC, Bolin Centre Database [data set], https://doi.org/10.17043/eriksson-2026-31pc-biomarker-1, 2026.

Fahl, K. and Stein, R.: Modern seasonal variability and deglacial/Holocene change of central Arctic Ocean sea-ice cover: New insights from biomarker proxy records, Earth Planet. Sci. Lett., 351–352, 123–133, https://doi.org/10.1016/j.epsl.2012.07.009, 2012.

Gustafsson, Ö., van Dongen, B. E., Vonk, J. E., Dudarev, O. V., and Semiletov, I. P.: Widespread release of old carbon across the Siberian Arctic echoed by its large rivers, Biogeosciences, 8, 1737–1743, https://doi.org/10.5194/bg-8-1737-2011, 2011.

Hörner, T., Stein, R., Fahl, K., and Birgel, D.: Post-glacial variability of sea ice cover, river run-off and biological production in the western Laptev Sea (Arctic Ocean) – A highresolution biomarker study, Quaternary Sci. Rev., 143, 133–149, https://doi.org/10.1016/j.quascirev.2016.04.011, 2016.

Hörner, T., Stein, R., and Fahl, K.: Paleo-sea ice distribution and polynya variability on the Kara Sea shelf during the last 12 ka, Arktos, 4, 11–16, https://doi.org/10.1007/s41063-018-0040-4, 2018.

Jakobsson, M., Mayer, L. A., Bringensparr, C., Castro, C. F., Mohammad, R., Johnson, P., Ketter, T., Accettella, D., Amblas, D., An, L., Arndt, J. E., Canals, M., Casamor, J. L., Chauché, N., Coakley, B., Danielson, S., Demarte, M., Dickson, M.-L., Dorschel, B., Dowdeswell, J. A., Dreutter, S., Fremand, A. C., Gallant, D., Hall, J. K., Hehemann, L., Hodnesdal, H., Hong, J., Ivaldi, R., Kane, E., Klaucke, I., Krawczyk, D. W., Kristoffersen, Y., Kuipers, B. R., Millan, R., Masetti, G., Morlighem, M., Noormets, R., Prescott, M. M., Rebesco, M., Rignot, E., Semiletov, I., Tate, A. J., Travaglini, P., Velicogna, I., Weatherall, P., Weinrebe, W., Willis, J. K., Wood, M., Zarayskaya, Y., Zhang, T., Zimmermann, M., and Zinglersen, K. B.: The International Bathymetric Chart of the Arctic Ocean Version 4.2., Sci. Data, 7, 176, https://doi.org/10.1038/s41597-020-0520-9, 2022.

Jensen, M. F., Nummelin, A., Nielsen, S. B., Sadatzki, H., Sessford, E., Risebrobakken, B., Andersson, C., Voelker, A., Roberts, W. H. G., Pedro, J., and Born, A.: A spatiotemporal reconstruction of sea-surface temperatures in the North Atlantic dur-

ing Dansgaard–Oeschger events 5–8, Clim. Past, 14, 901–922, https://doi.org/10.5194/cp-14-901-2018, 2018.

Karlsson, E., Gelting, J., Tesi, T., van Dongen, B., Andersson, A., Semiletov, I., Charkin, A., Dudarev, O., and Gustafsson, Ö.: Different sources and degradation state of dissolved, particulate, and sedimentary organic matter along the Eurasian Arctic coastal margin, Global Biogeochem. Cy., 30, 898–919, https://doi.org/10.1002/2015GB005307, 2016.

Keskitalo, K., Tesi, T., Bröder, L., Andersson, A., Pearce, C., Sköld, M., Semiletov, I. P., Dudarev, O. V., and Gustafsson, Ö.: Sources and characteristics of terrestrial carbon in Holocene-scale sediments of the East Siberian Sea, Clim. Past, 13, 1213–1226, https://doi.org/10.5194/cp-13-1213-2017, 2017.

Kremer, A., Stein, R., Fahl, K., Bauch, H., Mackensen, A., and Niessen, F.: A 190-ka biomarker record revealing interactions between sea ice, Atlantic Water inflow and ice sheet activity in eastern Fram Strait, Arktos, 4, 11–17, https://doi.org/10.1007/s41063-018-0052-0, 2018.

Köhler, P., Knorr, G., and Bard, E.: Permafrost thawing as a possible source of abrupt carbon release at the onset of the Bølling/Allerød, Nat. Commun., 5, 5520, https://doi.org/10.1038/ncomms6520, 2014.

Lambeck, K., Rouby, H., Purcell, A., Sun, Y., and Sambridge, M.: Sea level and global ice volumes from the Last Glacial Maximum to the Holocene, P. Natl. Acad. Sci. USA, 111, 15296–15303, https://doi.org/10.1073/pnas.1411762111, 2014.

Laskar, J., Robutel, P., Joutel, F., Gastineau, M., Correia, A.C.M., and Levrard, B.: A long-term numerical solution for the insolation quantities of the Earth, Astron. Astrophys., 428, 261–285, https://doi.org/10.1051/0004-6361:20041335, 2004.

Lin, T.-W., Tesi, T., Hefter, J., Grotheer, H., Wollenburg, J., Adolphi, F., Bauch, H. A., Nogarotto, A., Müller, J., and Mollenhauer, G.: Environmental controls of rapid terrestrial organic matter mobilization to the western Laptev Sea since the Last Deglaciation, Clim. Past, 21, 753–772, https://doi.org/10.5194/cp-21-753-2025, 2025.

Martens, J., Wild, B., Pearce, C., Tesi, T., Andersson, A., Bröder, L., O'Regan, M., Jakobsson, M., Sköld, M., Gemery, L., Cronin, T. M., Semiletov, I., Dudarev, O. V., and Gustafsson, Ö.: Remobilization of Old Permafrost Carbon to Chukchi Sea Sediments During the End of the Last Deglaciation, Global Biogeochem. Cy., 33, 2–14, https://doi.org/10.1029/2018GB005969, 2019.

Martens, J., Wild, B., Muschitiello, F., O'Regan, M., Jakobsson, M., Semiletov, I., Dudarev, O.V., and Gustafsson, Ö.: Remobilization of dormant carbon from Siberian-Arctic permafrost during three past warming events, Sci. Adv., 6, eabb6546, https://doi.org/10.1126/sciadv.abb6546, 2020.

Martens, J., Romankevich, E., Semiletov, I., Wild, B., van Dongen, B., Vonk, J., Tesi, T., Shakhova, N., Dudarev, O. V., Kosmach, D., Vetrov, A., Lobkovsky, L., Belyaev, N., Macdonald, R. W., Pieńkowski, A. J., Eglinton, T. I., Haghipour, N., Dahle, S., Carroll, M. L., Åström, E. K. L., Grebmeier, J. M., Cooper, L. W., Possnert, G., and Gustafsson, Ö.: CASCADE – The Circum-Arctic Sediment CArbon DatabasE, Earth Syst. Sci. Data, 13, 2561–2572, https://doi.org/10.5194/essd-13-2561-2021, 2021.

Martens, J., Wild, B., Semiletov, I., Dudarev, O.V., and Gustafsson, Ö.: Circum-Arctic release of terrestrial carbon varies between regions and sources, Nat. Commun., 13, 5858, https://doi.org/10.1038/s41467-022-33541-0, 2022.

Matsubara, F., Wild, B., Martens, J., Andersson, A., Wennström, R., Bröder, L., Dudarev, O.V., Semiletov, I., and Gustafsson, Ö.: Molecular-Multiproxy Assessment of Land-Derived Organic Matter Degradation Over Extensive Scales of the East Siberian Arctic Shelf Seas, Global Biogeochem. Cy., 36, e2022GB007428, https://doi.org/10.1029/2022GB007428, 2022.

Meyer, V., Hefter, J., Köhler, P., Tiedemann, R., Gersonde, R., Wacker, L., and Mollenhauer, G.: Permafrost-carbon mobilization in Beringia caused by deglacial meltwater runoff, sea-level rise and warming, 14, 085003, Environ. Res. Lett., https://doi.org/10.1088/1748-9326/ab2653, 2019.

Müller, J., Wagner, A., Fahl, K., Stein, R., Prange, M., and Lohmann, G.: Towards quantitative sea ice reconstructions in the northern North Atlantic: A combined biomarker and numerical modelling approach, Earth Planet. Sc. Lett., 306, 137–148, https://doi.org/10.1016/j.epsl.2011.04.011, 2011.

Muschitiello, F., O'Regan, M., Martens, J., West, G., Gustafsson, Ö., and Jakobsson, M.: A new 30 000-year chronology for rapidly deposited sediments on the Lomonosov Ridge using bulk radiocarbon dating and probabilistic stratigraphic alignment, Geochronology, 2, 81–91, https://doi.org/10.5194/gchron-2-81-2020, 2020.

Nicolas, A., Hefter, J., Grotheer, H., Tesi, T., Stein, R., Nogarotto, A., Alves, E. Q., and Mollenhauer, G.: Delivery of aged terrestrial organic matter to the Laptev Sea during the last deglaciation, Clim. Past, 21, 2579–2599, https://doi.org/10.5194/cp-21-2579-2025, 2025.

Nielsen, D. M., Dobrynin, M., Baehr, J., Razumov, S., and Grigoriev, M.: Coastal Erosion Variability at the Southern Laptev Sea Linked to Winter Sea Ice and the Arctic Oscillation, Geophys. Res. Lett., 47, e2019GL086876, https://doi.org/10.1029/2019GL086876, 2020.

Nielsen, D. M., Chegini, F., Maerz, J., Brune, S., Mathis, M., Dobrynin, M., Baehr, J., Brovkin, V., and Ilyina, T.: Reduced Arctic Ocean CO2 uptake due to coastal permafrost erosion, Nat. Clim. Change, https://doi.org/10.1038/s41558-024-02074-3, 2024.

Overduin, P. P., Schneider von Deimling, T., Meisner, F., Grigoriev, M. N., Ruppel, C., Vasilev, A., Lantuit, H., Juhls, H., and Westermann, S.: Submarine Permafrost Map in the Arctic Modeled Using1-D Transient Heat Flux (SuPerMAP), J. Geophys. Res.-Oceans, 124, 3487–3507, https://doi.org/10.1029/2018JC014675, 2019.

Overeem, I., Anderson, R. S., Wobus, C. W., Clow, G. D., Urban, F. E., and Matell, N.: Sea ice loss enhances wave action at the Arctic coast, Geophys. Res. Lett., 38, L17503, https://doi.org/10.1029/2011GL048681, 2011.

Pavia, F. J., Farmer, J. R., Gemery, L., Cronin, T. M., Treffkorn, J., and Farley, K. A.: Cosmic dust reveals dynamic shifts in central Arctic sea-ice cover-age over the past 30,000 years, Science, 390, 628–632, https://doi.org/10.1126/science.adv5767, 2025.

Reimer, P. J., Austin, W. E. N., Bard, E., Bayliss, A., Blackwell, P. G., Bronk Ramsey, C., Butzin, M., Cheng, H., Edwards, R. L., Friedrich, M., Grootes, P. M., Guilderson, T. P., Hajdas, I., Heaton, T. J., Hogg, A. G., Hughen, K. A., Kromer, B., Manning, S. W., Muscheler, R., Palmer, J. G., Pearson, C., van der Plicht, J., Reimer, R. W., Richards, D. A., Scott, E. M., Southon, J. R., Turney, C. S. M., Wacker, L., Adolphi, F., Büntgen, U., Capano, M., Fahrni, S. M., Fogtmann-Schulz, A., Friedrich, R., Köhler,

P., Kudsk, S., Miyake, F., Olsen, J., Reinig, F., Sakamoto, M., Sookdeo, A., and Talamo, S.: The IntCal20 Northern Hemisphere Radiocarbon Age Calibration Curve (0-55 kBP), Radiocarbon, 62, 725–757, https://doi.org/10.1017/RDC.2020.41, 2020.

Semiletov, I., Dudarev, O., Luchin, V., Charkin, A., Shin, K. H., and Tanaka, N.: The East Siberian Sea as a transition zone between Pacific-derived waters and Arctic shelf waters, Geophys. Res. Lett., 32, L10614, https://doi.org/10.1029/2005GL022490, 2005.

Sévellec, F., Fedorov, A. V., and Liu, W.: Arctic sea-ice decline weakens the Atlantic Meridional Overturning Circulation, Nat. Clim. Change, 7, 604–610, https://doi.org/10.1038/nclimate3353, 2017.

Shakun, J. D., Clark, P. U., He, F., Marcot, S. A., Mix, A. C., Zhengyu, L., Otto-Bliesner, B., Schmittner, A., and Bard, E.: Global warming preceded by increasing carbon dioxide concentrations during the last deglaciation, Nature, 484, 49–54, https://doi.org/10.1038/nature10915, 2012.

Schefuß, E., Eglinton, T. I., Spencer-Jones, C. L., Rullkötter, J., De Pol-Holz, R., Talbot, H. M., Grootes, P. M., and Schneider, R. R.: Hydrologic control of carbon cycling and aged carbon discharge in the Congo River basin, Nat. Geosci., 9, 687–690, https://doi.org/10.1038/ngeo2778, 2016.

Solomon, A.: Impact of latent heat release on polar climate, Geophys. Res. Lette., 33, https://doi.org/10.1029/2005GL025607, 2006.

Stein, R., Fahl, K., Schade, I., Manerung, A., Wassmuth, S., Niessen, F., and Nam, S.: Holocene variability in sea ice cover, primary production, and Pacific-Water inflow and climate change in the Chukchi and East Siberian Seas (Arctic Ocean), J. Quaternary Sci., 32, 362–379, https://doi.org/10.1002/jqs.2929, 2017.

Stranne, C., Jakobsson, M., and Björk, G.: Arctic Ocean perennial sea ice breakdown during the Early Holocene Insolation Maximum, Quaternary Sci. Rev., 92, 123–132, https://doi.org/10.1016/j.quascirev.2013.10.022, 2014.

Strauss, J., Schirrmesiter, L., Grosse, G., Fortier, D., Hugelius, G., Knoblauch, C., Romanovsky, V., Schädel, C., Schneider von Deimling, T., Schuur, E. A. G., Shmelev, D., Ulrich, M., and Veremeeva, A.: Deep Yedoma permafrost: A synthesis of depositional characteristics and carbon vulnerability, Earth Sci. Rev., 172, 75–86, https://doi.org/10.1016/j.earscirev.2017.07.007, 2017.

Strauss, J., Laboor, S., Schirrmeister, L., Fedorov, A. N., Fortier, D., Froese, D. G., Fuchs, M., Günther, F., Grigoriev, M. N., Harden, J. W., Hugelius, G., Jongejans, L. L., Kanevskiy, M. Z., Kholodov, A. L., Kunitsky, V., Kraev, G., Lozhkin, A. V., Rivkina, E., Shur, Y., Siegert, C., Spektor, V., Streletskaya, I., Ulrich, M., Vartanyan, S. L., Veremeeva, A., Walter A. K., Wetterich, S., Zimov, N. S., and Grosse, G.: Database of Ice-Rich Yedoma Permafrost Version 2 (IRYP v2), PANGAEA, https://doi.org/10.1594/PANGAEA.940078, 2022.

Taldenkova, E., Bauch, H. A., Stepanova, A., Ovsepyan, Y., Pogodina, I., Klyuvitkina, T., and Nikolaev, S.: Reprint of: Benthic and planktic community changes at the North Siberian margin in response to Atlantic water mass variability since last deglacial times, Mar. Micropaleontol., 99, 29–44, https://doi.org/10.1016/j.marmicro.2012.06.007, 2013.

Taylor, P. C., Cai, M., Hu, A., Meehl, J., Washington, W., and Zhang, G. J.: A Decomposition of Feedback Contributions to Polar Warming Amplification, J. Climate, 26, 7023–7043, https://doi.org/10.1175/JCLI-D-12-00696.1, 2013.

Tesi, T., Muschitiello, F., Smittenberg, R. H., Jakobsson, M., Vonk, J. E., Hill, P., Andersson, A., Kirchner, N., Noormets, R., Dudarev, O., Semiletov, I., and Gustafsson, Ö.: Massive remobilization of permafrost carbon during post-glacial warming, Nat. Commun., 7, 13653, https://doi.org/10.1038/ncomms13653, 2016.

Vaks, A., Mason, A. J., Breitenbach, S. F. M., Kononov, A. M., Osinzev, A. V., Rosensaft, M., Morshevsky, A., Gutareva, O. S., and Henderson, G. M.: Palaeoclimate evidence of vulnerable permafrost during times of low sea ice, Nature, 577, 221–225, https://doi.org/10.1038/s41586-019-1880-1, 2020.

Vandenberghe, J., Renssen, H., Roche, D. M., Goosse, H., Velichko, A. A., Gorbunov, A., and Levavasseur, G.: Eurasion permafrost instability constrained by reduced sea-ice cover, Quaternary Sci. Rev., 34, 16–23, https://doi.org/10.1016/j.quascirev.2011.12.001, 2012.

Vonk, J. E., Sánchez-Garcia, L., van Dongen, B. E., Alling, V., Kosmach, D., Charkin, A., Semiletov, I. P., Dudarev, O. V., Shakhova, N., Roos, P., Eglinton, T. I., Andersson, A., and Gustafsson, Ö.: Activation of old carbon by erosion of coastal and subsea permafrost in Arctic Siberia, Nature, 489, 137–140, https://doi.org/10.1038/nature11392, 2012.

Vonk, J. E., Fritz, M., Speetjens, N. J., Babin, M., Bartsch, A., Basso, L. S., Bröder, L., Göckede, M., Gustafsson, Ö., Hugelius, G., Irrgang, A. M., Juhls, B., Kuhn, M. A., Lantuit, H., Manizza, M., Martens, J., O'Regan, M., Suslova, A., Tank, S. E., Terhaar, J., and Zolkos, S.: The land-ocean Arctic carbon cycle, Nat. Rev. Earth Environ., 6, 86–105, https://doi.org/10.1038/s43017-024-00627-w, 2025.

Wild, B., Andersson, A., Bröder, L., Vonk, J., Hugelius, G., McClelland, J. W., Song, W., Raymond, P. A., and Gustafsson, Ö.: Rivers across the Siberian Arctic unearth the patterns of carbon release from thawing permafrost, P. Natl. Acad. Sci. USA, 116, 10280–10285, https://doi.org/10.1073/pnas.1811797116, 2019.

Winterfeld, M., Mollenhauer, G., Dummann, W., Köhler, P., Lembke-Jene, L., Hefter, J., McIntyre, C., Wacker, L., Kokfelt, U., and Tiedemann, R.: Deglacial mobilization of pre-aged terrestrial carbon from degrading permafrost, Nat. Commun., 9, 3666, https://doi.org/10.1038/s41467-018-06080-w, 2018.

Wu, J., Stein, R., Fahl, K., Syring, N., Seung-Il, N., Hefter, J., Mollenhauer, G., and Gilbert, W.: Deglacial to Holocene variability in surface water characteristics and major floods in the Beaufort Sea, Commun. Earth Environ., 1, 27, https://doi.org/10.1038/s43247-020-00028-z, 2020.

Wu, J., Mollenhauer, G., Stein, R., Köhler, P., Hefter, J., Fahl, K., Grotheer, H., Wei, B., and Nam, S.: Deglacial release of petrogenic and permafrost carbon from the Canadian Arctic impacting the carbon cycle, Nat. Commun., 13, 7172, https://doi.org/10.1038/s41467-022-34725-4, 2022.

Wu, J., Matsubara, F., Mollenhauer, G., Stein, R., Wei, B., Fahl, K., Xiao, X., and Gustafsson, Ö.: Geospatial patterns in terrestrial organic matter reactivity across four shelf seas spanning the Eurasian Arctic, Sci. Adv., 11, eadt6806, https://doi.org/10.1126/sciadv.adt6806, 2025.

Xiao, X., Fahl, K., and Stein, R.: Biomarker distributions in surface sediments from the Kara and Laptev seas (Arctic Ocean): indicators for organic-carbon sources

and sea-ice coverage, Quaternary Sci. Rev., 79, 40–52, https://doi.org/10.1016/j.quascirev.2012.11.028, 2013.

Xiao, X., Stein, R., and Fahl, K.: MIS 3 to MIS 1 temporal and LGM spatial variability in Arctic Ocean sea ice cover: Reconstruction from biomarkers, Paleooceanogr. Paleocl., 30, 969–983, https://doi.org/10.1002/2015PA002814, 2015.